solids

MDPI

Article

The Synergistic Effect of Fe-Based MOFs and HTPB on AP Decomposition in Solid Propellants

Qian Guo [1], Jie Wang [1], Yanchun Li [1,*] and Ramón Artiaga [1,2,*]

[1] School of Chemistry and Chemical Engineering, Nanjing University of Science and Technology, Nanjing 210097, China; qianguo@njust.edu.cn (Q.G.); jiewang@njust.edu.cn (J.W.)
[2] Centro de Investigación en Tecnologías Navales e Industriales, Campus Industrial de Ferrol, University of A Coruña, 15403 Ferrol, Spain
* Correspondence: liyanchun@njust.edu.cn (Y.L.); ramon.artiaga@udc.es (R.A.)

Abstract: Many factors and their mutual interaction between catalysts and AP/HTPB composite solid propellant induce the complexity in the combustion. Among them, we prepared two Fe-based MOFs as catalysts and investigated their catalytic effects and mechanism on the decomposition AP, HTPB and AP/HTPB complex by TG-DSC and TG-IR. The results show that both Fe-based MOFs exhibit catalytic effects on the decomposition of all samples. Specifically, in the AP/HTPB/MOFs composite system, a synergistic effect between MOFs and HTPB is observed, substantially accelerating the decomposition of both AP and HTPB, which makes the HTD temperature of AP advance approximately 100 °C, beyond what would be expected from each component acting independently. Mechanistic studies demonstrate that Fe_2O_3@C produced by the decomposition of Fe-based MOF uses the decomposition products of HTPB as a bridge to accelerate the overflow of NH_3 on the surface of AP, thereby allowing AP to decompose rapidly at a lower temperature and also accelerating the decomposition of HTPB. Moreover, its influence on the combustion performance of AP-based composite propellants was studied and the combustion rate increased by 20%. This research provides the new directions for designing and applying of Fe-based MOFs materials in HTPB-based solid propellent.

Keywords: Fe-based MOF; AP/HTPB; catalyst; propellants

Academic Editor: Michael A. Beckett

Received: 13 April 2025
Revised: 16 May 2025
Accepted: 27 May 2025
Published: 3 June 2025

Citation: Guo, Q.; Wang, J.; Li, Y.; Artiaga, R. The Synergistic Effect of Fe-Based MOFs and HTPB on AP Decomposition in Solid Propellants. *Solids* **2025**, *6*, 27. https://doi.org/10.3390/solids6020027

1. Introduction

In the field of solid propellant technology, the pursuit of high-performance composite propellants has emerged as a cornerstone of research endeavors, driven by their indispensable role across a spectrum of applications, including aerospace, missiles, and rocket systems [1,2]. The quest for these advanced propellants is fueled by the need for enhanced energy density, improved combustion efficiency, and reliable performance under diverse operational conditions. Among the various components of solid propellants, ammonium perchlorate (AP) and hydroxyl-terminated polybutadiene (HTPB) are widely utilized as oxidizers and binders, respectively. AP undergoes thermal decomposition to liberate oxygen, which is crucial for sustaining the combustion reaction [3,4]. The fuel binder is responsible for providing structural integrity to the propellant grain by encapsulating and immobilizing the particulate oxidizers or metals within a cohesive matrix [5,6]. Furthermore, the interaction between AP and HTPB, facilitated by appropriate additives and processing techniques, determines the overall characteristics of the propellant, such as burning rate, heat release, and pressure generation [7,8]. The thermal decomposition characteristics of these components directly influence the combustion performance and energy release of the

propellant. Consequently, enhancing the decomposition efficiency of both AP and HTPB through innovative catalytic strategies is a crucial research direction aimed at optimizing propellant performance [9,10].

However, although substantial research efforts have been dedicated to the decomposition behavior of ammonium perchlorate and its burning rate, the decomposition of fuel binder has unfortunately received relatively scant attention [11,12]. Any suitable additives that can enhance the heat of combustion or the pyrolysis rate of fuel binders could potentially elevate the overall burning rate of the propellant [13,14]. Hence, it is imperative to investigate comprehensively the decomposition of AP/HTPB in the presence of combustion catalysts, which involves dissecting the effects of catalysts on the thermal decomposition behaviors of AP, HTPB, and their blends. This approach enables a nuanced understanding of how catalysts interact with individual components, facilitating the design of tailored catalytic strategies that optimize the overall propellant performance.

In recent years, with the continuous drive to enhance the combustion performance of AP/HTPB solid propellants, iron compounds including iron nanoparticles [15], iron oxide [16–18], Fe_2O_3-based composite materials [19,20], ferrocene-based compounds [21–23], etc. have been used as propellant combustion catalysts and demonstrated promising catalytic activities. In particular, Fe-based nanocatalysts show catalytic activity superior to their bulk catalysts due to their high surface-to-volume ratios and enhanced reactivity [24]. Among the emerging nanomaterial, metal organic frameworks (MOFs) materials have garnered considerable interest as combustion catalysts for solid propellants and energetic materials, due to their excellent catalytic performance and complex and diverse structural characteristics [25–28]. The utilization of MOFs as catalysts offers the potential to finely tune the decomposition profiles of AP and HTPB, thereby optimizing the overall combustion performance of composite solid propellants. Moreover, by focusing on understanding the intricate interactions between these catalysts and propellant components, it becomes possible to gain deeper insights into the underlying mechanisms governing propellant combustion [29,30]. This in turn enables the unlocking of greater potential for enhancing the overall efficiency and performance of solid propellants, ultimately paving the way for the development of next-generation solid propellants with superior performance characteristics.

In this study, two Fe-based MOFs were synthesized as the AP, HTPB and AP/HTPB thermal decomposition catalysts, and the structure characteristics of the materials were determined by scanning electron microscope (SEM), transmission electron microscope (TEM), X-ray photoelectron spectroscopy (XPS), X-ray Diffraction (XRD), and Brunauer-Emmett-Teller (BET) analysis. Additionally, the catalytic performance of these materials was systematically investigated via thermogravimetric-differential scanning calorimetry (TG-DSC). Meanwhile, the gas products generated during the reaction process were examined through thermogravimetric-Infrared spectroscopy (TG-IR), which furnished valuable information regarding the decomposition mechanisms and intermediate species formed. On this basis, the decomposition mechanism of AP/HTPB in the presence of MOFs was studied, which will help us understand the catalytic mode of action of Fe-based catalysts and provide a new direction for the design and application of new Fe-based MOFs in propellants.

2. Experimental

2.1. Materials

All the reagents and solvents used in the experiment were of analytical grade and were not further purified. Ammonium perchlorate (NH_4ClO_4, AP, 250~420 μm) powder was obtained from Dalian Gaojia Chemical Industry Co., Ltd., (Dalian, Liaoning, China). Hydroxy-terminated polybutadiene (HTPB) was obtained from Zibo OILONG Chemical

Industry Co., Ltd., (Zibo, Shandong, China). (HTPB, ($\overline{Mn}$): 3800–4600, hydroxyl group content: 0.47–0.53 mmol/g). 1,4-benzene dicarboxylic acid (1,4-BDC) was from Tianjin Heowns Biochemical Technology Co., Ltd., (Tianjin, China). $FeCl_3 \cdot 6H_2O$ was from Guangdong Guanghua Sci-Tech Co., Ltd., (Guangzhou, China). N,N-dimethylformamide (DMF) was from Meryer Chemical Technology Co., Ltd., (Shanghai, China). Isophorone diisocyanate (IPDI), triphenyl bismuth (TPB) and methanol were purchased from Nanjing Juyou Scientific Equipment Co., Ltd., (Nanjing, Jiangsu, China). Cetyltrimethylammonium bromide (CTAB) was from Nanjing WanQing chemical Glass ware & Instrument Co., Ltd., (Nanjing, Jiangsu, China).

2.2. Preparation of MOF-235 and Fe-MOF

MOF-235 was synthesized by a solvothermal method as reported previously with minor modification [31]. 1.08 g CTAB was dissolved into 50 mL of a DMF/EtOH (*v*:*v*, 1:1) mixture by sonication. Then, 1.2 g 1,4-BDC was added, stirred uniformly and mixed with 50 mL of another DMF/EtOH (*v*:*v*, 1:1) solution containing 2.6 g $FeCl_3 \cdot 6H_2O$. The mixture was hermetically sealed in a 100 mL Teflon-lined stainless-steel reactor, and the reactor was kept at 110 °C for 12 h. After the reaction was complete, the mixture was centrifuged with methanol several times and dried in a vacuum drying oven at 70 °C.

The preparation method of Fe-MOF was similar to that of MOF-235, except that the mixture of DMF and ethanol was replaced by methanol and was only stirred at ambient conditions instead of using the solvothermal method (Scheme 1).

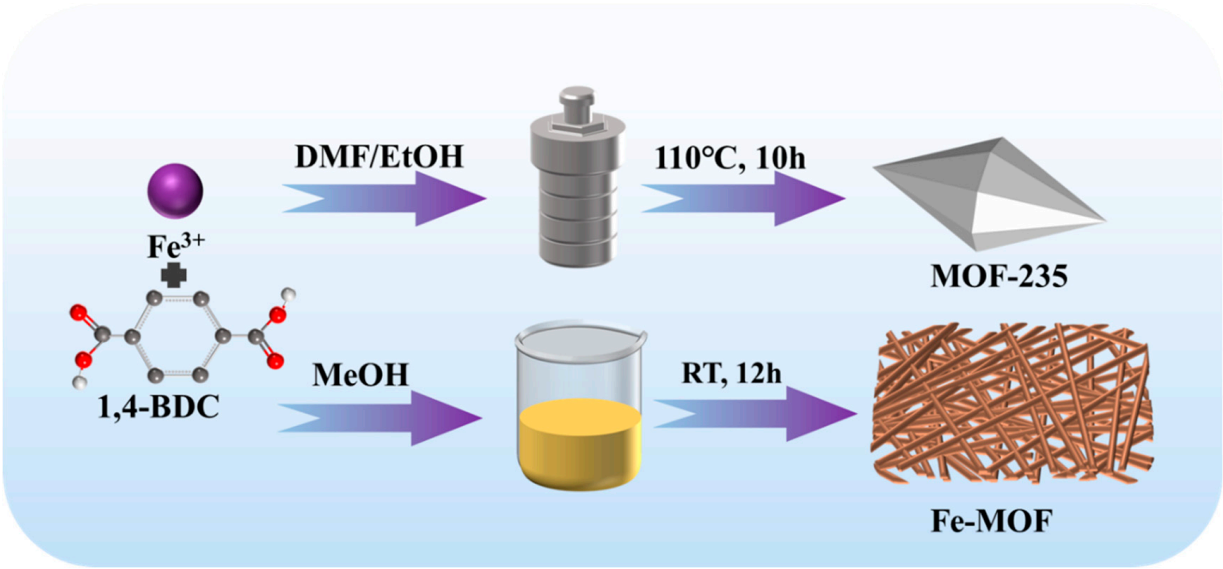

Scheme 1. Schematic diagram of the preparation of Fe-based MOFs.

2.3. Preparation of the AP/MOF, HTPB/MOF, AP/HTPB/MOF and AP/HTPB Mixture

MOF/AP samples were prepared by incorporation of Fe-based MOFs into AP at a mass ratio of 2%, followed by mixing and grinding.

MOF/HTPB, MOF/AP/HTPB and AP/HTPB mixtures were prepared. HTPB was used as a binder, isophorone diisocyanate (IPDI) and triphenyl bismuth (TPB) were used as the was used as curing agent and catalysts, respectively, for crosslinking of HTPB. The detailed formulations of the prepared mixtures are displayed on Table 1. All components were sequentially incorporated into a beaker and the mixing process was kept for about 30 min. Then the prepared slurry was poured into a polytetrafluoroethylene (PTFE) mold, subjected to a partial vacuum for 30 min to eliminate voids and bubbles in the mixture. Finally, the sample was placed into an oven at 60 °C for 4 days to get the fully cured composites.

Table 1. The dosage of each component used in the mixtures.

Samples	AP/g	HTPB/g	IPDI/g	TPB/g	MOF/g
MOF/AP	5	0	0	0	0.1
MOF/HTPB	0	5	0.486	0.006	0.1
MOF/AP/HTPB	3.75	1.139	0.11	0.001	0.1
AP/HTPB	3.75	1.139	0.11	0.001	0

2.4. Preparation of AP Based Solid Propellant

According to the actual production process, the components were uniformly mixed and then cured in an oven at 60 °C for seven days. The formula of AP based solid propellant is shown in Table 2.

Table 2. The dosage of each component used in the AP based solid propellant.

Samples	HTPB	DOS/TPB/IPDI	Al	AP	MOF
AP/Al/HTPB	10.3%	4.7%	17%	68%	0
MOF/AP/Al/HTPB	10.3%	4.7%	17%	66%	2%

The prepared propellant samples were coated four times with an 8% polyvinyl alcohol coating solution, followed by a combustion test.

2.5. Characterization

Surface morphology of Fe-based MOFs was observed by scanning electron microscopy (SEM, Hitachi Regulus 8100, Tokyo, Japan) and transmission electron microscope (TEM, FEI Talos F200X G2, Waltham, MA, USA). The crystal structure of the samples was studied by X-ray diffraction (XRD, Bruker D8, Advance, Billerica, MA, USA) with Cu Kα radiation (40 kV and 40 mA). The valence of elements of two MOFs were examined by X-ray photoelectron spectroscopy (XPS, Thermo Scientific K-Alpha, Waltham, MA, USA). Binding energies were corrected for surface charging by referring to the band energy of the C 1s peak at 284.8 eV. The pore size distributions and the Brunauer-Emmett-Teller (BET) surface area analysis were studied with nitrogen adsorption/desorption at 77 K by means of a Micromeritics 3Flex surface area analyzer (Micromeritics, Norcross, GA, USA). Prior to N_2 adsorption analysis, samples were degassed under vacuum at 100 °C for 12 h to remove physically adsorbed species. The catalytic effect of two MOFs on AP, HTPB and AP/HTPB thermal decomposition was studied by thermogravimetry-differential scanning calorimetry (TG-DSC, TGA/DSC3+, METTLER TOLEDO, Temecula, CA, USA). The heating rate was 10 °C/min, and the N_2 flow rate was 25 mL/min. A Netzsch infrared spectrometer (STA-2500, Selb, Bavaria, Germany) was attached to the gas outlet of the TG-DSC apparatus to detect the gaseous products evolved from the degradation processes.

Ignition experimental conditions: Propellant samples of the same quality were prepared into propellant strips with 5 × 5 × 30 mm, and the propellant strips were used as ignition samples. A nickel-chromium wire (0.3 mm in diameter) was placed in the middle of the section of the propellant strips and ignited in the air atmosphere. A nickel-chromium (0.3 mm in diameter) wire was wound around a section of the sample, and ignited in the air atmosphere and the combustion process of the sample was recorded. Each sample was tested 3 times.

3. Results and Discussion

3.1. Characterization of Fe-MOF and MOF-235

The MOF-235 was synthesized by the solvothermal method and the Fe-MOF was obtained by replacing the DMF/EtOH mixture by MeOH and using room temperature.

Figure 1 shows the SEM images of MOF-235 and Fe-MOF. For MOF-235, a well-crystallized octahedral morphology is observed, which shows a relatively uniform size distribution with crystals of about 3–4.5 μm, with few exceptions. However, the SEM image of Fe-MOF exhibits a complex, intertwined fibrous structure and is different from the morphologies of the previously reported Fe-based MOF [32]. According to the TEM images displayed in Figure 1d, Fe-MOF presents acicular structures, with significant variations in size, ranging from nanoscale dimensions to larger microscale lengths.

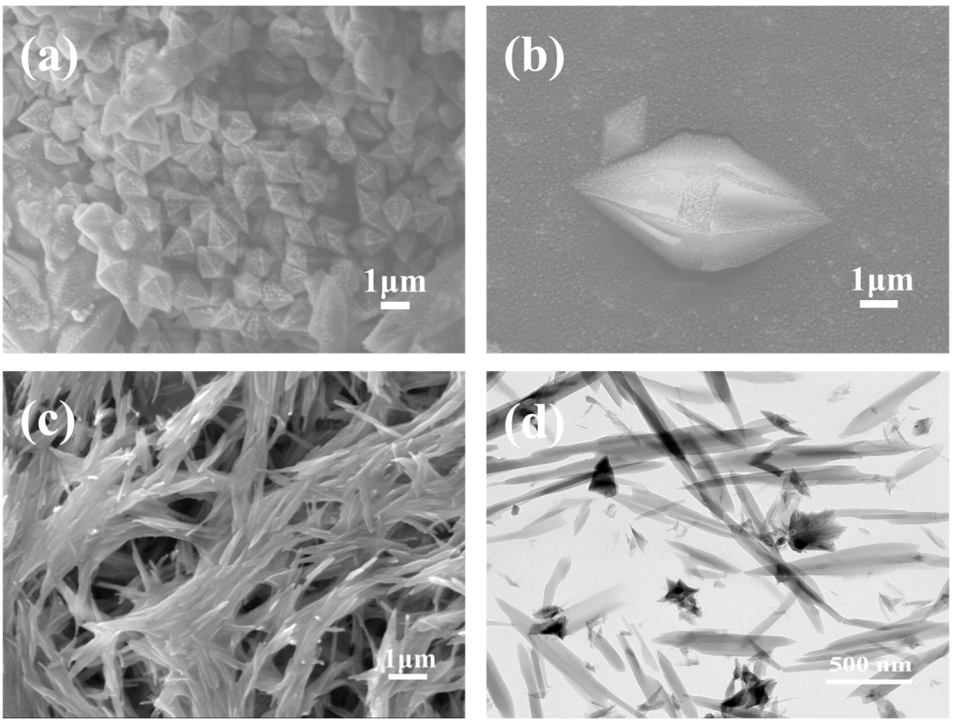

Figure 1. The SEM images of MOF-235 (**a**,**b**); the SEM and TEM images of Fe-MOF (**c**,**d**).

The crystallographic structure of MOF-235 and Fe-MOF was further characterized by X-ray diffraction (XRD). As shown in Figure 2a, the main diffraction peaks of MOF-235 are located at 2θ = 9.7, 12.6, 19 and 22, corresponding to the crystal plane family of (101), (102), (202), (311), respectively, which are consistent with previously reported experimental data of MOF-235 as well as simulated data [33,34], thus confirming the successful synthesis of MOF-235. Conversely, the XRD plot of Fe-MOF indicates the existence of a variety of different phases or crystal structures in the sample, as it has multiple independent diffraction peaks in the range of 10–30° (2θ), consistent with the TEM result.

The composition and valence state of catalyst's surface elements are of paramount importance in the process of catalytic adsorption. Therefore, XPS was employed to determine the surface composition and elemental valence states of the two MOF materials (Figure 2b). The high-resolution XPS spectrum of Fe(2p) reveals binding energy peaks at 711.8 eV and 725.2 eV, which are attributed to Fe 2p3/2 and Fe 2p1/2, respectively. The peak separation, namely, $\Delta = 2p_{1/2} - 2p_{3/2} = 13.4$ eV, which closely matches the values reported for Fe_2O_3 [31]. Moreover, the spectra also show that the patterns of Fe-MOF are similar to those of MOF-235, suggesting that the chemical environment of Fe^{3+} is identical in both MOFs.

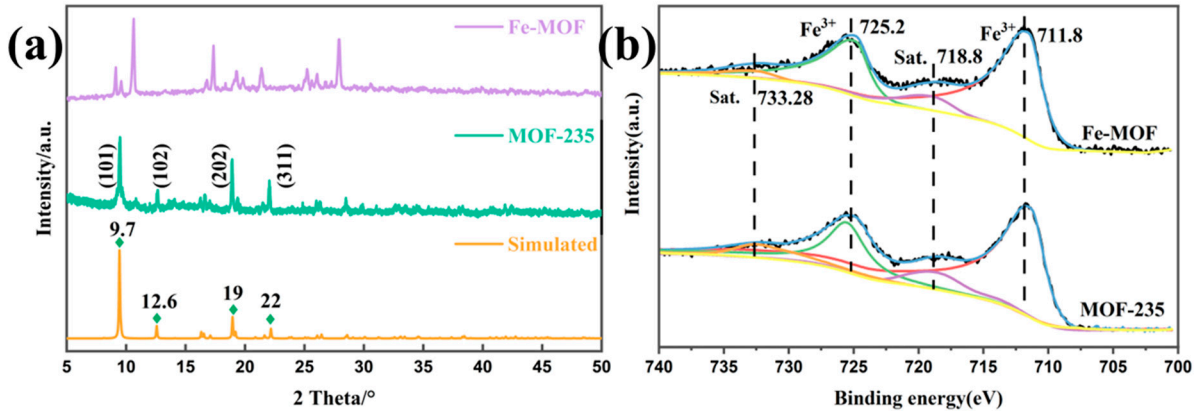

Figure 2. (**a**) XRD results and (**b**) XPS spectrum of MOF-235 and Fe-MOF.

To further investigate the specific surface area and porous structure of the as-synthesized samples, N_2 adsorption-desorption isotherms of MOF-235 and Fe-MOF were measured at 77 K, as presented in Figure 3. The BET surface areas are determined as 911 and 8 m^2/g, respectively, for MOF-235 and Fe-MOF. The adsorption-desorption curves of the two MOFs show different behaviors; MOF-235 exhibits a typical type I isotherm, a signature characteristic of microporous materials, while Fe-MOF shows a type II isotherm, which is indicative of non-porous materials [35,36]. Moreover, the insets graph of Figure 3 as pore size distribution curves have shown the data points between the 5 nm to 60 nm range for both MOFs. The average pore size and pore volume (BJH adsorption) resulted in MOF-235 to 3.10 nm, 0.255 cm^3/g and Fe-MOF to 12.8 nm, 0.014 cm^3/g.

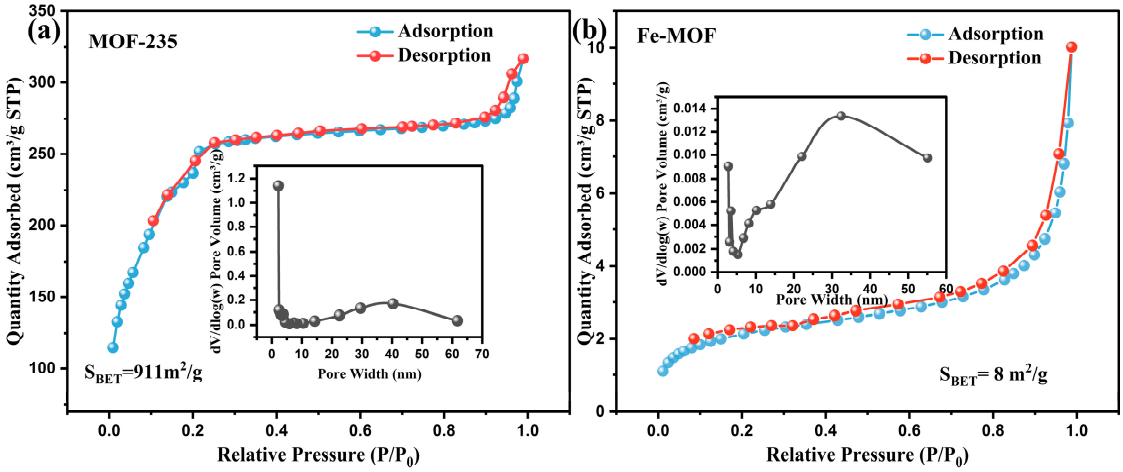

Figure 3. N_2 adsorption-desorption isotherms and pore size distribution curves of (**a**) MOF-235, (**b**) Fe-MOF.

In order to understand the decomposition and combustion mechanisms of composite systems containing catalysts, decomposition of the catalysts is the starting point. Investigation on pyrolysis behavior of MOFs is essential to evaluate their catalytic mechanism on the decomposition of AP/HTPB. Both iron-based MOFs were subjected to thermogravimetric analysis (TGA) to evaluate their thermal stability, as shown in Figure 4.

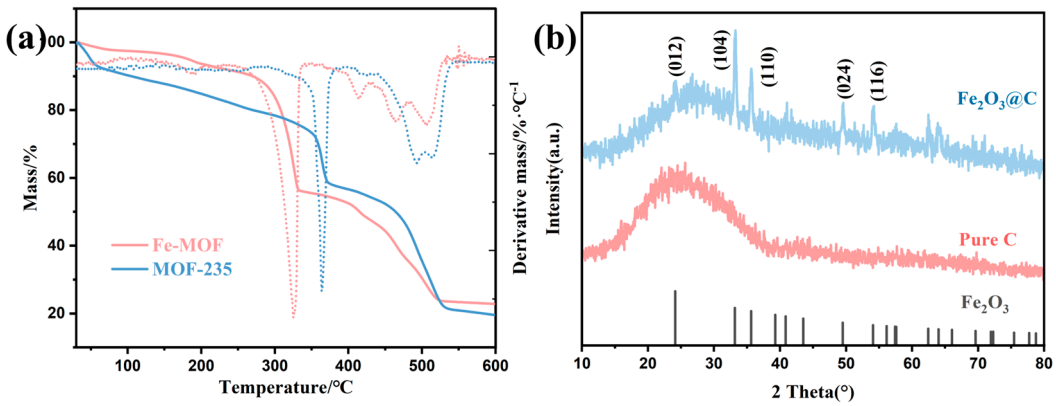

Figure 4. (**a**) TG-DTG curves of Fe-MOF and MOF-235 (**b**) XRD results of the residue of Fe-based MOFs.

The TG-DTG curves show that the main decomposition peak occurs above 300 °C, which means the samples have good thermal stability. Initial mass losses can be attributed to evaporation of free water and residual solvents. Other mass losses are presumably related to decarboxylations and decomposition of the framework structure. Above 550 °C, the weight basically remains unchanged, which indicates that most of the organic matter had already decomposed at 550 °C. A 20% residue was obtained, whose analysis by XRD revealed that it was composed of Fe_2O_3@C, in line with previous studies [37].

3.2. The Catalytic Effect of Fe-MOF and MOF-235 on the Thermal Decomposition of Ammonium Perchlorate

The performance of AP decomposition plays a decisive role in the combustion process of propellants [38]. To investigate the catalytic performance of MOF-235 and Fe-MOF on the thermal decomposition of AP, TG-DSC experiments were conducted at a heating rate of 10 °C·min^{-1}. Then, the activation energy was calculated by Kissinger method. The results are illustrated in Figure 5.

Three main processes are identified in the AP DSC curves: an endothermic peak at 244.6 °C, attributable to the crystalline phase transition from orthorhombic to cubic symmetry; followed by the exothermic peaks corresponding to low-temperature decomposition (LTD) at 297.5 °C and high temperature decomposition (HTD) at 437.3 °C, respectively. This result is in accordance with previous reports [39–41].

Upon addition of the catalyst, the thermal decomposition process of AP undergoes a notable change, which is mainly manifested in the advancement of HTD peaks of AP decomposition, but shows a negligible influence on the crystalline phase transition and LTD peaks. This behavior may be related to the relatively high thermal stability of MOFs. MOFs don't produce catalytically active products at the LTD temperature, and, thus, they do not significantly affect the AP LTD stage. However, as temperature increases, MOFs begin to decompose and exhibit a catalytic effect on AP. Specifically, the HTD peak temperature of Fe-MOF/AP and MOF-235/AP shifts to 399.2 °C and 384 °C, respectively, representing reductions of 38.1 °C and 53.3 °C with respect to the pristine AP HTD temperature. In addition, the apparent heat release during the high-temperature thermal decomposition increases to 923.2 J·g^{-1} and 1042.8 J·g^{-1} respectively.

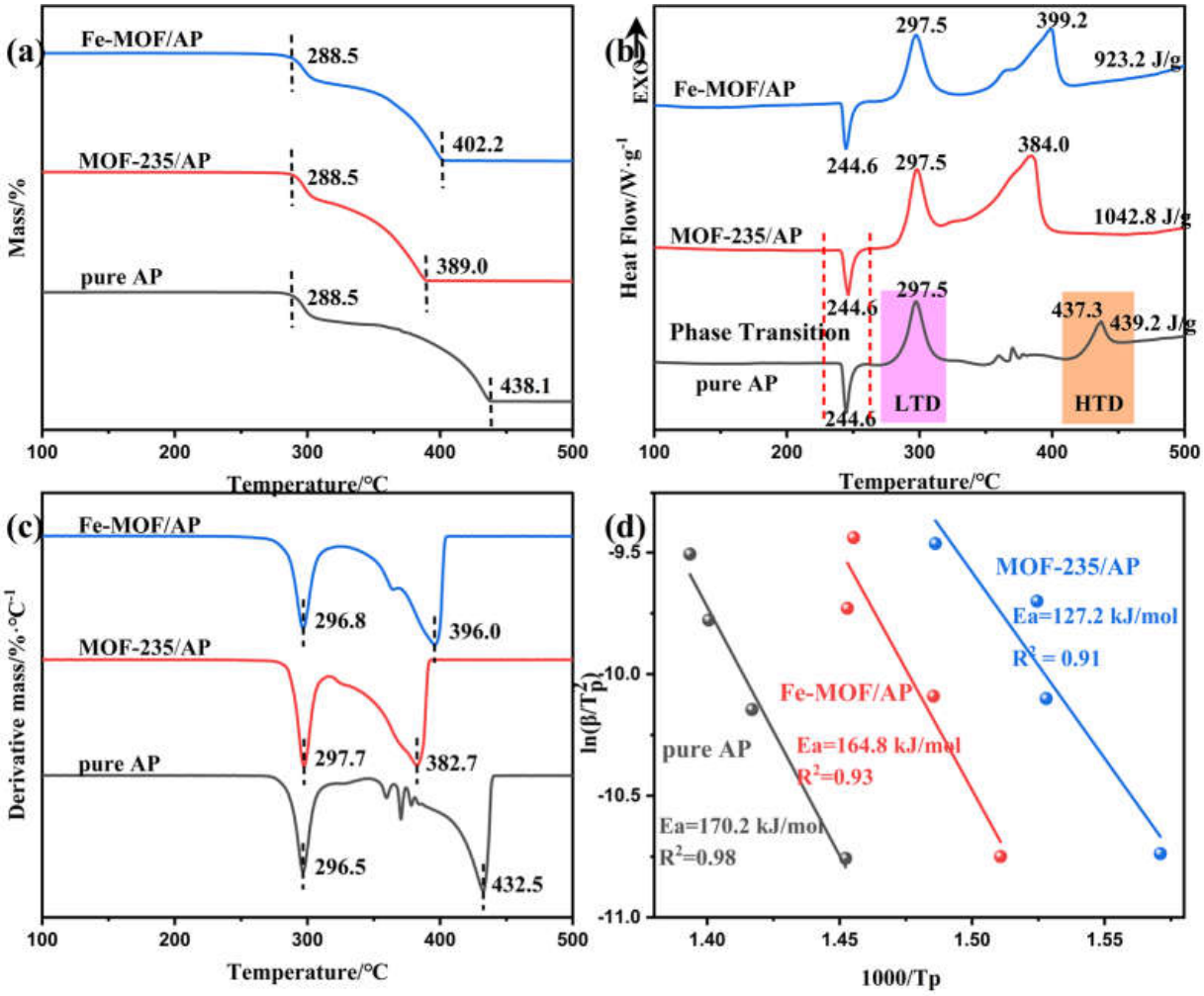

Figure 5. TG (**a**), DSC (**b**) and DTG (**c**) curves obtained from pure AP, Fe-MOF/AP and MOF-235/AP. Plot of ln(β/Tp2) versus 1/Tp obtained from AP, Fe-MOF/AP and MOF-235/AP, where the scatter points represent the experimental data and the line denote the results of the linear fit (**d**).

In general, the catalyst reduces activation energy (*Ea*) of the AP decomposition process, which accelerates the rate at which it decomposes when heated. In this study, catalysts mainly acted on the second stage of AP decomposition, so the kinetic parameters corresponding to HTD stage were calculated by Kissinger equation [42]. As shown in Table 3 and Figure 5d, the calculated activation energy for pure AP is 170.2 kJ·mol^{-1}; which decreases to 164.8 kJ·mol^{-1} with Fe-MOF catalysis and further reduces to 127.2 kJ·mol^{-1} with MOF-235 catalysis. These results mean that both Fe-MOF and MOF-235 were catalytically active for the thermal decomposition of AP. According to the previous results [25], Fe_2O_3@C can accelerate the electron transfer between O_2 and O_2^- during the HTD stage, thus promoting the decomposition of AP.

Table 3. LTD temperature (T_{LTD}), HTD temperature (T_{HTD}), heat release (ΔH) and activation energy (*Ea*) of the mixtures of AP and catalysts.

Samples	T_{LTD} (°C)	T_{HLD} (°C)	ΔH (J·g^{-1}) at the Second Stage	*Ea* (kJ·mol^{-1}) at the Second Stage
Pure AP	297.5	437.3	439.2	170.2
MOF-235/AP	297.5	384.0	1042.8	127.2
Fe-MOF/AP	297.5	399.2	923.2	164.8

3.3. The Catalytic Effect of Fe-MOF and MOF-235 on Thermal Decomposition of HTPB

Apart from the oxidizer, the binder is also a crucial component in solid propellants. Hydroxyl-terminated polybutadiene (HTPB) is a long-chain, cross-linked polymer with a high molecular weight that has served as the binder in solid propellants, and typically acts as a fuel, which gets oxidized in the combustion processes, and it has been pointed out that the oxidative degradation of HTPB is increased by catalysts [14,43]. However, some literature shows that MOF materials exhibit high oxidation resistance to polymers [44,45], so the effect of MOFs on HTPB was investigated by TG-DSC, with results presented in Figure 6.

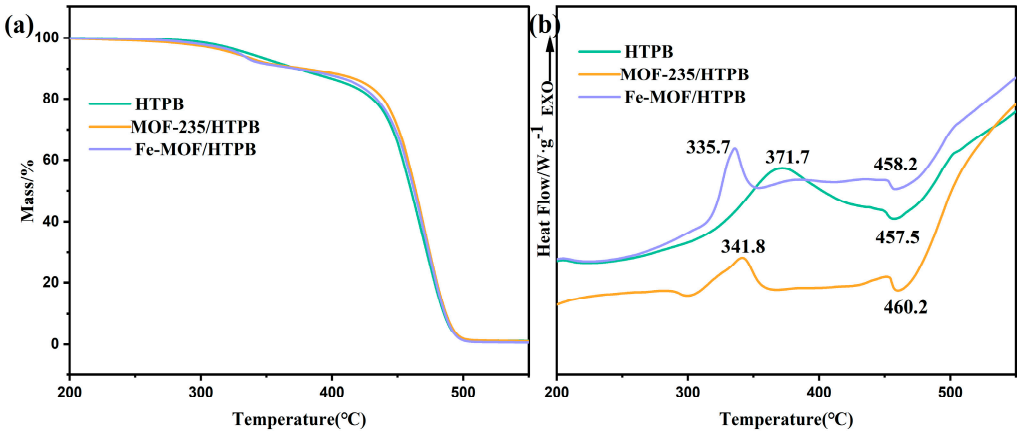

Figure 6. TG (**a**), DSC (**b**) curves of HTPB, MOF-235/HTPB and Fe-MOF/HTPB.

The TG-DSC curve of HTPB presented in Figure 6 exhibits two distinct stages: a net exothermic stage and a net endothermic stage. The exothermic peak is observed at 371.7 °C, primarily attributed to the exothermic cross-linking cyclization and the endothermic depolymerization of HTPB. The second stage predominantly involves the degradation of the residual polymer structure, with a corresponding endothermic peak appearing at 458 °C [46]. The volatilization process continued until the residue practically disappeared.

With the incorporation of Fe-MOF and MOF-235, the overall thermal degradation profile of HTPB remained largely unaffected, as evidenced by the similarity in TGA curves of the three samples, indicating that the MOFs do not significantly change the decomposition mechanism of HTPB.

However, it can be seen from the DSC curves that the addition of Fe-MOF and MOF-235 mainly affects the exothermic stage of HTPB, while the effect on the subsequent degradation of the polymer structure seems negligible. Specifically, there is a reduction in exothermic peak temperature by 36 °C and 30 °C for Fe-MOF and MOF-235 respectively, along with a decrease in heat release, indicating that MOFs could facilitate the depolymerization of HTPB in the first stage, so that the first stage of degradation is concentrated in a narrower temperature range. Considering the fact that both MOFs decompose during the first stage of HTPB, it could be hypothesized that the decomposition intermediate of MOFs and/or its decomposition product plays a critical role to enhance the depolymerization of HTPB [47].

3.4. The Catalytic Effect of Fe-MOF and MOF-235 on Thermal Decomposition of AP/HTPB Composite

According to the results presented above, it can be observed that MOFs exhibit a catalytic effect on the decomposition of AP and HTPB. To further explore the catalytic influence of MOFs on the decomposition of AP/HTPB mixtures, the TG-DSC experiments were conducted in the 30–600 °C range of temperature. The results are displayed on Figure 7 and Table 3.

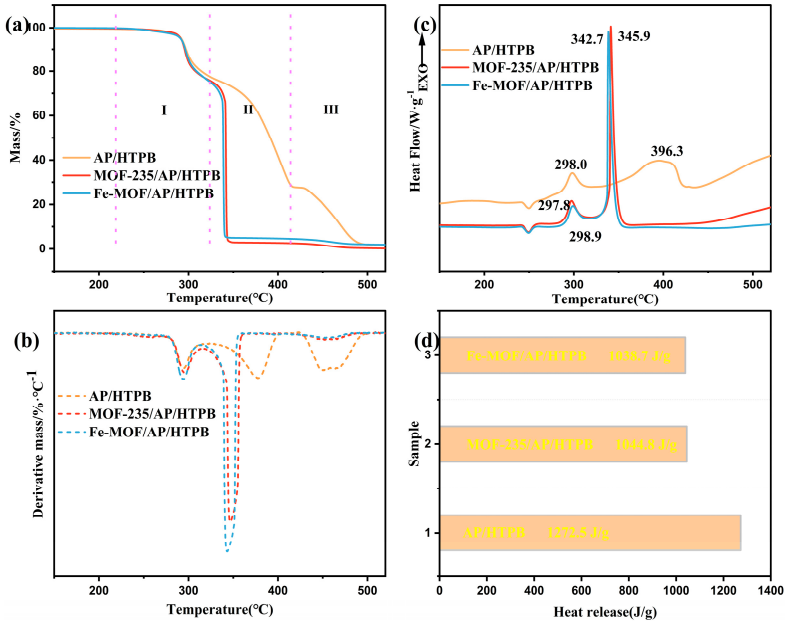

Figure 7. TG (**a**), DTG (**b**) and DSC (**c**) curves of AP/HTPB, MOF-235/AP/HTPB, Fe-MOF/AP/HTPB. Heat release during the high temperature decomposition of AP/HTPB without and with catalysts (**d**).

The decomposition process of the AP/HTPB complex, as illustrated in Figure 7a,c, occurs in three distinct stages (I, II, III), with complete degradation occurring at about 500 °C. The initial stage primarily involves the low-temperature decomposition of AP, with a peak temperature around 300 °C. At this temperature, HTPB remains stable and does not undergo decomposition. In Stage II, as the temperature increases, AP begins to decompose at elevated temperatures while some degradation of HTPB is observed; this transition is completed at approximately 410 °C. Subsequently, the Stage III mainly involves the decomposition of residual HTPB and is completed at about 500 °C.

In the MOFs/AP/HTPB composite system, following the introduction of Fe-MOF/MOF-235 catalysts, no significant effect is observed on the low-temperature decomposition corresponding to the first stage across samples in all samples.

However, in second stage, a decrease in the decomposition temperature and an acceleration of the decomposition rate were observed. The peak temperatures of the MOF-235/AP/HTPB and Fe-MOF/AP/HTPB shift to lower values, with decreases of 50.4 and 53.7 °C, respectively. Moreover, the sample decomposes completely within a very narrow temperature range, with heat release concentrated. The mass loss of the Stage II of these composites increases by approximately 24% compared to that of AP/HTPB, suggesting that a substantial amount of HTPB decomposes during this stage. The heat loss, peak temperature, and heat release at different stages of the decomposition process are listed in Table 4.

Table 4. The mass loss of different stages, the peak temperature and heat release of stage II.

Samples	Mass Loss/%			T_{II} (°C)	Heat Release of Stage II ($J \cdot g^{-1}$)
	I	II	III		
AP/HTPB	24.25	47.78	25.82	396.3	1272.5
MOF-235/AP/HTPB	23.30	74.05	2.38	345.9	1044.8
Fe-MOF/AP/HTPB	23.58	71.84	2.62	342.7	1038.7

A comparison of the AP/HTPB curve with those of the pure compounds makes it possible to establish that the first stage of decomposition of the mixture corresponds,

practically unchanged, to that of AP (Figure 8). Similarly, the last stage of decomposition of the mixture, which starts at approximately 410 °C, corresponds to HTPB. It can be seen that the amount of mass involved in last stage is similar to the HTPB content of the mixture. On the contrary, the second stage of the mixture seems to encompass the HTPB process delimited with vertical lines and the AP degradation occurring above 305 °C. There is an obvious interaction between the two compounds since they are mixed, the joint process is completed about 40 °C lower than in the case of AP alone. Nevertheless, the decomposition behavior of HTPB in this composite system closely resembles that of pure HTPB, suggesting that the thermal degradation process of AP does not disrupt that of HTPB and HTPB continues to decompose according to its inherent thermal degradation mechanism.

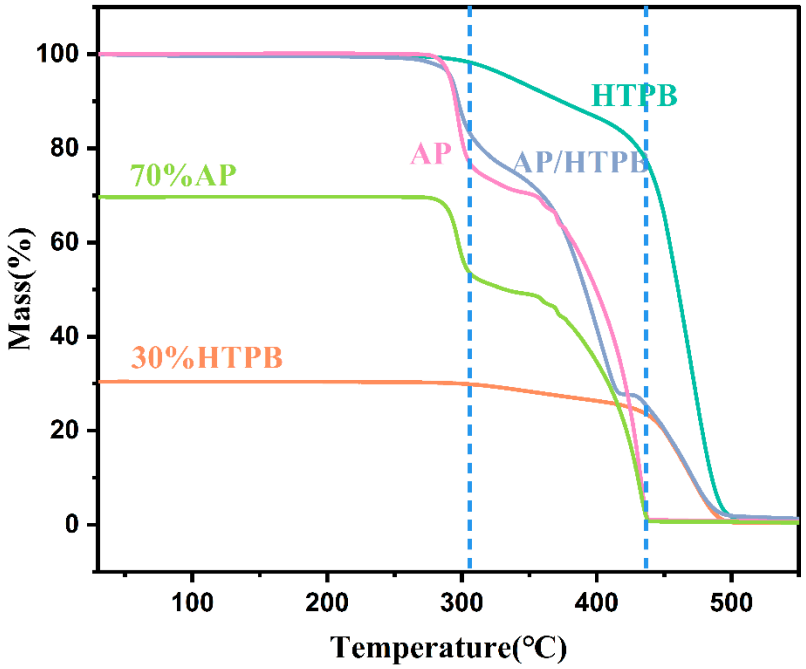

Figure 8. The TG curves of AP, HTPB and AP/HTPB.

Moreover, a comparative analysis of thermal decomposition results among AP/MOFs, HTPB/MOFs, AP/HTPB and AP/HTPB/MOFs reveals that both Fe-MOF/MOF-235 and HTPB exert a promoting effect on AP decomposition. Meanwhile, MOFs enhance HTPB's breakdown during exothermic stages, while AP does not seem to influence thermal degradation of HTPB. Astonishingly, when these three components form a composite system together, their combined effects substantially accelerate both AP and HTPB decompositions beyond what would be expected from each component acting independently, which indicates that the MOFs and HTPB have a synergistic effect on the decomposition of the systems as a whole.

3.5. TG-IR Results

In order to further investigate the specific mechanism of incorporation of MOFs materials on the catalysis of AP/HTPB, the gas-phase products in the course of the thermal decomposition process of AP/HTPB catalyzed by MOFs were monitored by TG-IR, and as a comparison, the gas products of AP/HTPB were also tested. The results are shown in Figure 9.

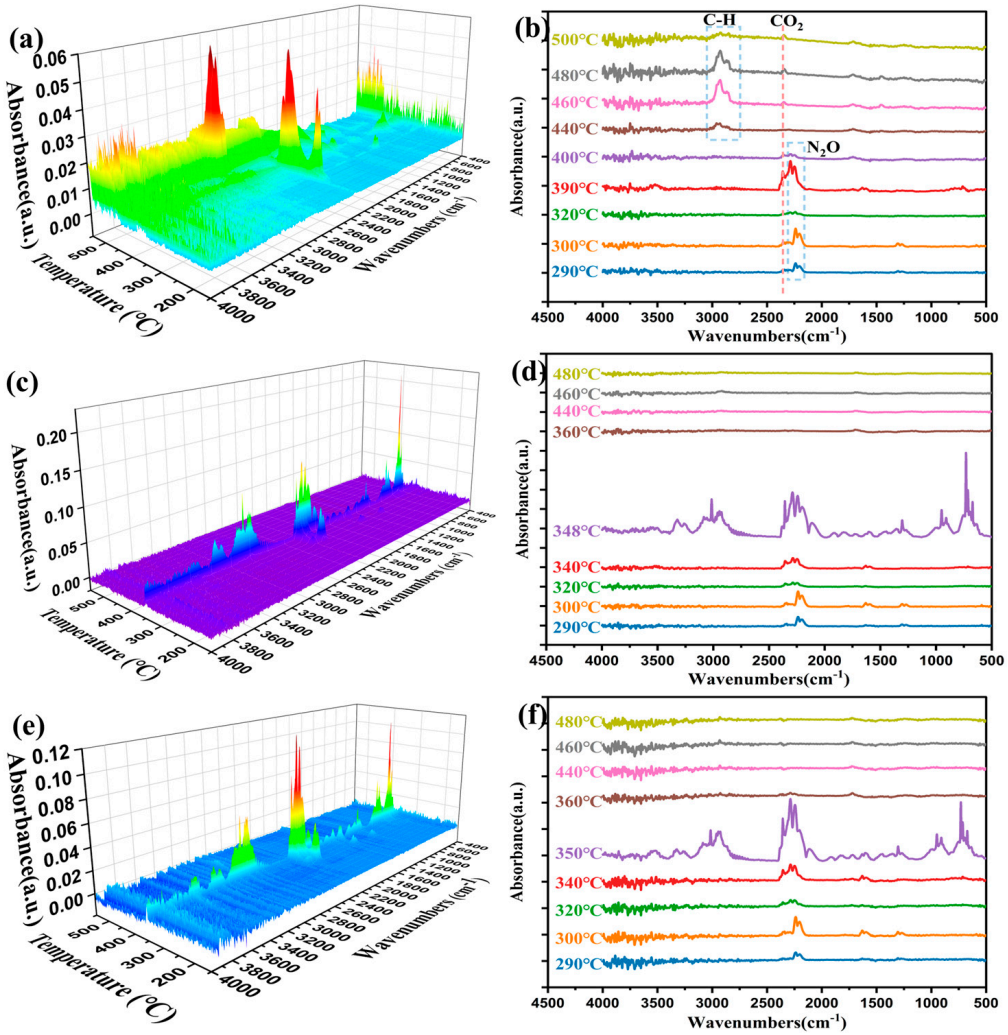

Figure 9. FTIR spectra obtained from the gases evolved from TGA experiments with the samples: AP/HTPB (**a**,**b**), Fe-MOF/AP/HTPB (**c**,**d**), and MOF-235/AP/HTPB (**e**,**f**).

For the AP/HTPB, the monitored gas product first appears at 290 °C, the main characteristic band position is 2238 cm^{-1}, and corresponding gas product is N_2O. As the reaction temperature rises, the characteristic peak intensity of N_2O gradually increases and then decreases, corresponding to the completion of Stage I of AP/HTPB [48]. Trace CO_2 characteristic bands were also detected, indicating that the MOF is undergoing decomposition in this stage. As temperature increases, the stage II of AP/HTPB begins, accompanied by an enhancement of the characteristic band of CO_2 (2356 cm^{-1}) and NO_2 (1631/1597 cm^{-1}), which reaches its maximum at around 390 °C, and finally disappears around 410 °C, representing the decomposition of both AP and HTPB, with AP nearly fully decomposed. Then, at about 440 °C, a characteristic band appears at 2932/2866 cm^{-1}, which corresponds to the stretching vibration of C-H, indicating that the residual HTPB decomposition [49], which concludes by 500 °C.

However, the decomposition of AP/HTPB catalyzed by Fe-MOF or MOF-235 exhibits rather disparate gas generation behaviors. As can be discerned from Figure 9c–f, during the initial stage I at around 300 °C, the detected gas characteristic band aligns with that of AP/HTPB but with a slight enhancement in intensity. As the temperature increases to the range of 340–350 °C, a remarkably distinct gas generation behavior emerges compared to AP/HTPB. Notably, at around 350 °C, in addition to the characteristic peaks corresponding to N_2O and CO_2, multiple characteristic peaks are detected, indicating substantial decomposition of HTPB at this stage, and the reactions occur between gaseous products of AP

and HTPB. Subsequently, after reaching 360 °C, only a weak CO_2 characteristic peak can be observed, indicating the ending of decomposition. Moreover, Figure 10 presents the FTIR results of gas products obtained during thermal decomposition of AP/HTPB/MOF-235 and AP/HTPB/Fe-MOF at the peak temperature. The principal decomposition products are CO_2, N_2O, C_2H_2, C_2H_4, C_4H_6, HCN, etc., [50]. It can be speculated that HTPB participates in the thermal decomposition reaction. On the one hand, large hydrocarbon molecules break down into small hydrocarbon molecules; on the other hand, the large and small hydrocarbon molecules are capable of reacting with the decomposition products of AP to generate CO, CO_2, HCN.

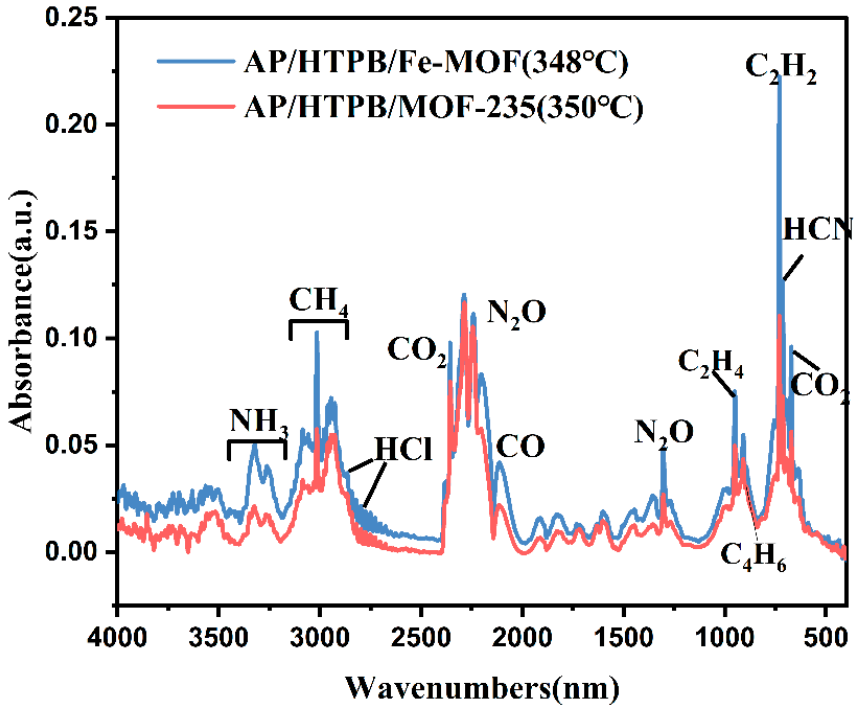

Figure 10. FTIR curve of gas products in the thermal decomposition of AP/HTPB/Fe-MOF and AP/HTPB/MOF-235 at the peak temperature.

The results presented above demonstrate that the existence of MOFs and HTPB jointly enhance the decomposition of AP. The synergistic effect of the MOFs and HTPB affects the decomposition and reaction process of the composite system.

As shown in Figure 11, the corresponding catalytic mechanism is proposed. Due to the thermal stability of Fe-based MOFs and HTPB, they don't affect the LTD of AP. As temperature rises, the MOFs decompose and generate the Fe_2O_3@C, which promotes the HTD of AP by accepting the electron of AP, accelerating the electron transfer and reducing the activation energy. Moreover, it causes the first stage of HTPB to be concentrated and release the gaseous products, i.e., 1,3-butadiene, and CO_2, which provide an acid atmosphere for NH_3 desorption, causing the acceleration of AP. Meanwhile, the heat release of AP also facilitates the pyrolysis of HTPB, thus forming a positive cycle and making the quick decomposition of AP and HTPB.

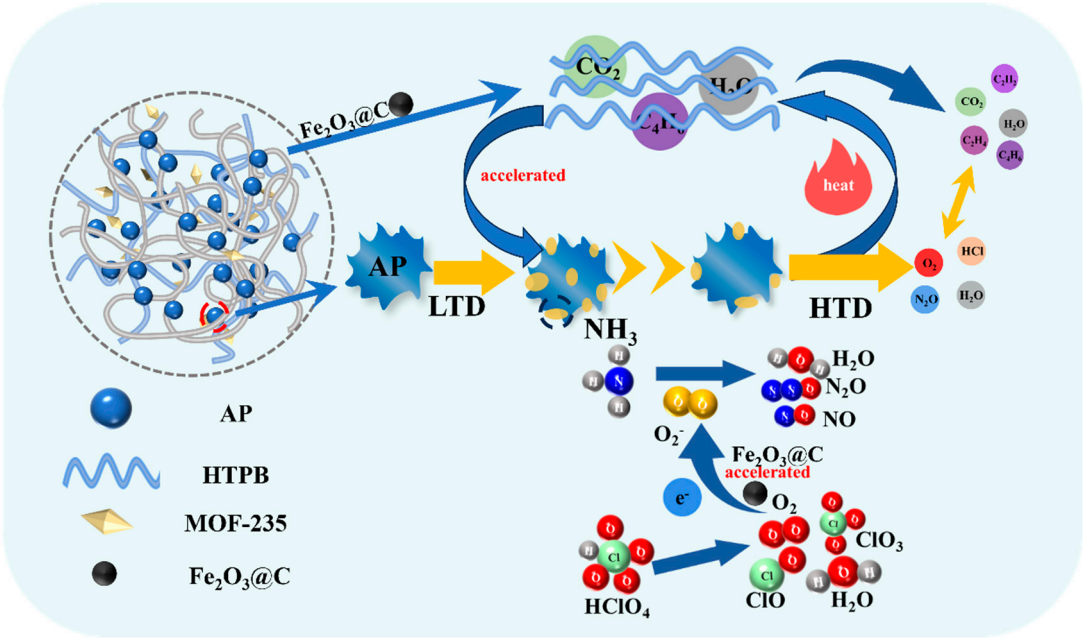

Figure 11. The catalytic mechanism of AP/HTPB decomposition on Fe-based MOF.

3.6. Study on Combustion Catalytic Performance

For investigating the impact of catalytic on combustibility of composite solid propellants, the burning behaviors of the propellants were captured, and shown in Figure 12. The propellants strips with catalysts had faster combustion rates, and both MOFs exhibited essentially the same efficiency in enhancing the combustion rate, by 20%, compared with the propellant strips without catalyst. Moreover, it was found that the burning rate enhancement for both MOFs was similar with burning rate enhancements reported in the literature for Fe_2O_3, suggesting the catalytic effects of both MOFs were similar to that of Fe_2O_3. This is consistent with the results of the previous thermal analysis.

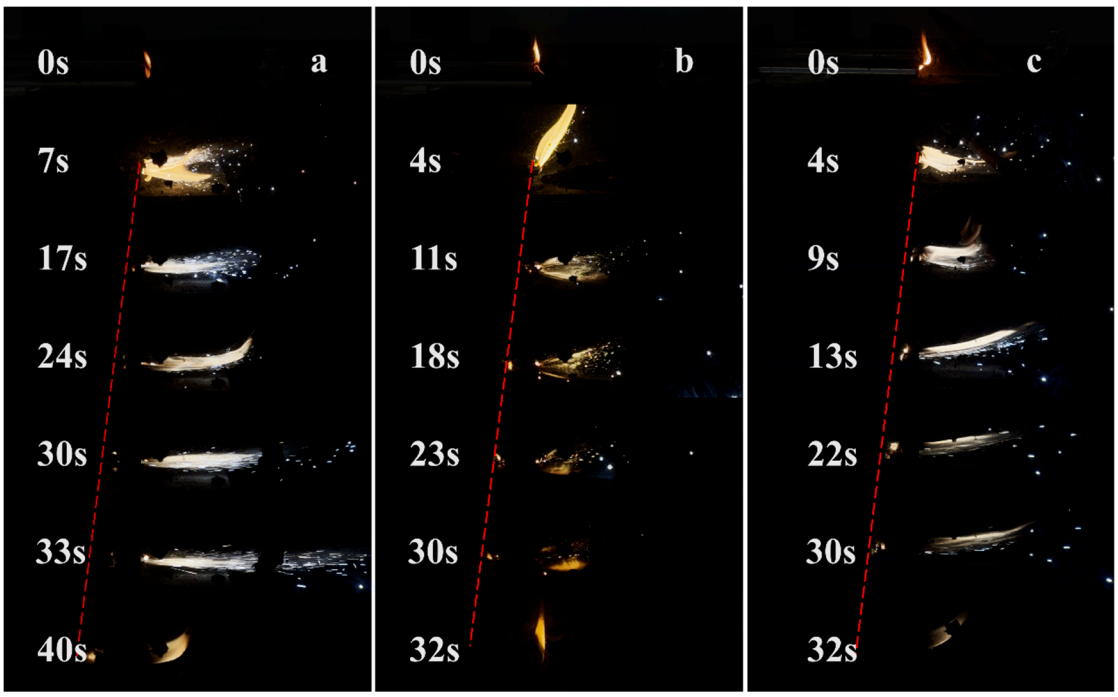

Figure 12. Combustion process of (**a**) AP/HTPB, (**b**) Fe-MOF/AP/HTPB, (**c**) MOF-235/AP/HTPB.

4. Conclusions

In summary, the present study demonstrates the significant catalytic effects of two Fe-based MOFs (MOF-235 and Fe-MOF) on the thermal decomposition of AP and HTPB composites in solid propellants. The results revealed both MOFs decreased the activation energy of AP, which was beneficial in reducing the thermal decomposition temperature and increasing the heat release from AP. Additions of Fe-MOF and MOF-235 results in increases in AP heat release from 439.2 to 923.2 J/g and 1042.8 J/g, respectively, and decrease in HTD temperature from 437.2 to 399.2 °C and 384.0 °C, respectively. In particular, a synergistic effect is observed on decomposition of AP/HTPB/MOFs composites, which made the HTD temperature of AP decrease from 437.2 to 342.7 °C. The TG-IR results indicated that this synergistic effect, which is attributed to the combined action of MOFs and HTPB, jointly enhance the decomposition of AP and accelerate the pyrolysis of HTPB, forming a positive cycle. Furthermore, MOFs enhances the combustion performance of AP-based solid propellants by improving the thermal decomposition behavior of AP, and the combustion rate increased by 20%. Overall, the findings of this study contribute to a deeper understanding of the catalytic mechanisms of Fe-based MOFs in solid propellant formulations and provide valuable insights for the design and application of new catalysts in this field.

Author Contributions: Investigation and writing-original draft, Q.G.; writing-review and editing, J.W.; supervision, R.A.; supervision and funding acquisition, Y.L. All authors have read and agreed to the published version of the manuscript.

Funding: This work was funded by Southwest Technology and Engineering Research Institute Funding, HDH5923A0204.

Data Availability Statement: Data is contained within the article.

Conflicts of Interest: The authors declare no conflict of interest.

References

1. Zhou, Q.; Jin, B.; Chu, S.; Peng, R. Farrow-derived layered porous carbon aerogel for AP catalytic thermal Decomposition. *Inorg. Chem. Front.* **2021**, *8*, 2798–2808. [CrossRef]
2. Chen, J.; He, S.; Liu, Y.; Qiao, Z.; Huang, B.; Li, X.; Hao, Q.; Huang, H.; Yang, G. Highly active catalysts based on 3D hierarchically ordered porous carbon with entrapped Fe_2O_3 nanoparticles for the thermal decomposition of ammonium Perchlorate. *Appl. Surf. Sci.* **2021**, *538*, 148148. [CrossRef]
3. Manash, A.; Kumar, P. Comparison of burn rate and thermal decomposition of AP as oxidizer and PVC and HTPB as fuel binder based composite solid Propellants. *Def. Technol.* **2019**, *15*, 227–232. [CrossRef]
4. Dolgoborodov, A.; Streletskii, A.; Shevchenko, A.; Vorobieva, G.; Val'Yano, G. Thermal decomposition of mechanoactivated ammonium Perchlorate. *Thermochim. Acta* **2018**, *669*, 60–65. [CrossRef]
5. Sinha, Y.K.; Sridhar, B.T.N.; Santhosh, M. Thermal decomposition study of HTPB solid fuel in the presence of activated charcoal and Paraffin. *J. Therm. Anal. Calorim.* **2015**, *119*, 557–565. [CrossRef]
6. Beck, W.H. Pyrolysis studies of polymeric materials used as binders in composite propellants: A Review. *Combust. Flame* **1987**, *70*, 171–190. [CrossRef]
7. Dong, G.; Liu, H.; Deng, L.; Yu, H.; Zhou, X.; Tang, X.; Li, W. Study on the interfacial interaction between ammonium perchlorate and Hydroxyl-terminated polybutadiene in solid propellants by molecular dynamics Simulation. *E-Polymers* **2022**, *22*, 264–275. [CrossRef]
8. Liang, J.; Nie, J.; Zhang, H.; Guo, X.; Yan, S.; Han, M. Interaction Mechanism of Composite Propellant Components under Heating Conditions. *Polymers* **2023**, *15*, 2485. [CrossRef]
9. Trache, D.; Klapötke, T.M.; Maiz, L.; Abd-Elghany, M.; DeLuca, L.T. Recent advances in new oxidizers for solid rocket Propulsion. *Green Chem.* **2017**, *19*, 4711–4736. [CrossRef]
10. Chen, T.; Hu, Y.-W.; Zhang, C.; Gao, Z.-J. Recent progress on transition metal oxides and Carbon-supported transition metal oxides as catalysts for thermal decomposition of ammonium Perchlorate. *Def. Technol.* **2021**, *17*, 1471–1485. [CrossRef]

11. Dennis, C.; Bojko, B. On the combustion of heterogeneous AP/HTPB composite propellants: A Review. *Fuel* **2019**, *254*, 115646. [CrossRef]
12. Chaturvedi, S.; Dave, P.N. Solid propellants: AP/HTPB composite Propellants. *Arab. J. Chem.* **2019**, *12*, 2061–2068. [CrossRef]
13. Kohga, M. Burning Characteristics and Thermochemical Behavior of AP/HTPB Composite Propellant Using Coarse and Fine AP Particles. *Propellants Explos. Pyrotech.* **2011**, *36*, 57–64. [CrossRef]
14. Vellaisamy, U.; Biswas, S. Effect of metal additives on neutralization and characteristics of AP/HTPB solid Propellants. *Combust. Flame* **2020**, *221*, 326–337. [CrossRef]
15. Styborski, J.A.; Scorza, M.J.; Smith, M.N.; Oehlschlaeger, M.A. Iron Nanoparticle Additives as Burning Rate Enhancers in AP/HTPB Composite Propellants. *Propellants Explos. Pyrotech.* **2015**, *40*, 253–259. [CrossRef]
16. Xu, H.; Wang, X.; Zhang, L. Selective preparation of nanorods and micro-octahedrons of Fe2O3 and their catalytic performances for thermal decomposition of ammonium perchlorate. *Powder Technol.* **2008**, *185*, 176–180. [CrossRef]
17. Padwal, M.B.; Varma, M. Thermal decomposition and combustion characteristics of HTPB-coarse AP composite solid propellants catalyzed with Fe2O3. *Combust. Sci. Technol.* **2018**, *190*, 1614–1629. [CrossRef]
18. Zhang, Y.; Liu, X.; Nie, J.; Yu, L.; Zhong, Y.; Huang, C. Improve the catalytic activity of α-Fe2O3 particles in decomposition of ammonium perchlorate by coating amorphous carbon on their Surface. *J. Solid State Chem.* **2011**, *184*, 387–390. [CrossRef]
19. Dave, P.N.; Sirach, R. NiZnFe2O4: A potential catalyst for the thermal decomposition of AP and burn rate modifier for AP/HTPB based Propellants. *J. Therm. Anal. Calorim.* **2022**, *147*, 10999–11011. [CrossRef]
20. Wang, Y.; Yang, X.; Lu, L.; Wang, X. Experimental study on preparation of LaMO3 (M = Fe, Co, Ni) nanocrystals and their catalytic Activity. *Thermochim. Acta* **2006**, *443*, 225–230. [CrossRef]
21. Abdin, Z.; Wang, L.; Yu, H.; Saleem, M.; Akram, M.; Abbasi, N.; Khalid, H.; Sun, R.; Chen, Y. Ferrocene-based polyethyleneimines for burning rate Catalysts. *New J. Chem.* **2016**, *40*, 3155–3163. [CrossRef]
22. Amin, B.U.; Yu, H.; Wang, L.; Nazir, A.; Fahad, S.; Haq, F.; Mahmood, S.; Liang, R.; Uddin, M.A.; Lin, T. Recent advances on Ferrocene-based compounds and polymers as a burning rate catalysts for Propellants. *J. Organomet. Chem.* **2020**, *921*, 121368. [CrossRef]
23. Feng, H.; Liu, X.; Li, Y.; Ma, X.; Yan, Q.; Zhao, F. Novel powder catalysts of Ferrocene-based metal-organic framework and their catalytic performance for thermal decomposition of ammonium Perchlorate. *Powder Technol.* **2022**, *397*, 117035. [CrossRef]
24. Chaturvedi, S.; Dave, P.N. A review on the use of nanometals as catalysts for the thermal decomposition of ammonium Perchlorate. *J. Saudi Chem. Soc.* **2013**, *17*, 135–149. [CrossRef]
25. Yang, Y.; Bai, Y.; Zhao, F.; Yao, E.; Yi, J.; Xuan, C.; Chen, S. Effects of metal organic framework Fe-BTC on the thermal decomposition of ammonium Perchlorate. *RSC Adv.* **2016**, *6*, 67308–67314. [CrossRef]
26. Feng, C.; Ye, B.; Cheng, W.; Shi, S.; Zhao, F.; An, C.; Wang, J. Microflower-like Fe-Co-MOF with enhanced catalytic performance for decomposition of ammonium perchlorate and combustion of ammonium perchlorate-based composite Propellants. *Case Stud. Therm. Eng.* **2024**, *56*, 104281. [CrossRef]
27. Wang, S.; Ye, B.; An, C.; Song, X.; Wang, J. Synergistic catalysis of ZIF-67@CNTOH in thermal decomposition of ammonium Perchlorate. *J. Mater. Sci.* **2020**, *55*, 4646–4655. [CrossRef]
28. Shi, Y.; Chang, Q.; Song, T.; Yin, M.; Zhang, L.; Cao, X.; Wei, Z.; Cao, X. Energetic Metal-organic framework based on multinuclear clusters of Cu(II) and Fe(III) and its catalytic action on thermal decomposition of solid propellant components (RDX, HMX, CL-20 and AP). *Chem. Eng. J.* **2023**, *479*, 147394. [CrossRef]
29. Tan, B.; Yang, X.; Dou, J.; Duan, B.; Lu, X.; Liu, N. Research progress of EMOFs-based burning rate catalysts for solid Propellants. *Front. Chem.* **2022**, *10*, 1032163. [CrossRef]
30. Jojic, I.; Brewster, M.Q. Condensed-Phase Chemical Interaction Between Ammonium Perchlorate and Hydroxy-Terminated Polybutadiene. *J. Propuls. Power* **1998**, *14*, 575–576. [CrossRef]
31. Li, Y.; Hou, G.; Yang, J.; Xie, J.; Yuan, X.; Yang, H.; Wang, M. Facile synthesis of MOF 235 and its superior photocatalytic capability under visible light Irradiation. *RSC Adv.* **2016**, *6*, 16395–16403. [CrossRef]
32. Guo, W.; Sun, W.; Lv, L.-P.; Kong, S.; Wang, Y. Microwave-Assisted Morphology Evolution of Fe-Based Metal–Organic Frameworks and Their Derived Fe_2O_3 Nanostructures for Li-Ion Storage. *ACS Nano* **2017**, *11*, 4198–4205. [CrossRef] [PubMed]
33. Deng, Q.; Feng, S.; Hui, P.; Chen, H.; Tian, C.; Yang, R.; Xu, Y. Exploration of Low-cost microporous Fe(III)-based organic framework as anode material for potassium-ion Batteries. *J. Alloys Compd.* **2020**, *830*, 154714. [CrossRef]
34. Simonsson, I.; Gärdhagen, P.; Andrén, M.; Tam, P.L.; Abbas, Z. Experimental investigations into the irregular synthesis of iron(III) terephthalate metal–organic frameworks MOF-235 and MIL-101. *Dalton Trans.* **2021**, *50*, 4976–4985. [CrossRef] [PubMed]
35. Alothman, Z. A Review: Fundamental Aspects of Silicate Mesoporous Materials. *Materials* **2012**, *5*, 2874–2902. [CrossRef]
36. Khalfaoui, M.; Knani, S.; Hachicha, M.; Lamine, A. New theoretical expressions for the five adsorption type isotherms clasified by BET based on statistical physics Treatment. *J. Colloid Interface Sci.* **2003**, *263*, 350–356. [CrossRef]
37. Qiao, Y.; Li, N.; Dong, M.; Jia, P.; Ma, C.; Zhang, T.; Jiao, T. MOF-Derived MnO/C Nanocomposites for High-Performance Supercapacitors: 23. *Nanomaterials* **2022**, *12*, 4257. [CrossRef]

38. Feng, C.; Ye, B.; An, C.; Zhang, F.; Hong, Z.; Wang, J. Preparation of functionalized GO coordination compound and its catalytic performance for thermal decomposition of ammonium Perchlorate. *J. Mater. Sci.* **2021**, *56*, 19599–19613. [CrossRef]
39. Majeed, M.A.; Lei, X.; Xu, J.; Jiang, A.; Arif, M.; Song, C.; Cheng, L.; Zhang, Z.; Li, Y.; Zhang, W. Physiochemical aspect of different CuO catalyst surface to APC thermochemical Transformation. *Surf. Interfaces* **2024**, *45*, 103826. [CrossRef]
40. Wang, S.; Ye, B.; An, C.; Wang, J.; Li, Q.; Guo, H.; Zhang, J. Exploring the Coordination Effect of GO@MOF-5 as Catalyst on Thermal Decomposition of Ammonium Perchlorate. *Nanoscale Res. Lett.* **2019**, *14*, 345. [CrossRef]
41. Vyazovkin, S.; Wight, C.A. Kinetics of Thermal Decomposition of Cubic Ammonium Perchlorate. *Chem. Mater.* **1999**, *11*, 3386–3393. [CrossRef]
42. Zhou, P.; Zhang, S.; Ren, Z.; Tang, X.; Zhang, K.; Zhou, R.; Wu, D.; Liao, J.; Zhang, Y.; Huang, C. In Situ Cutting of Ammonium Perchlorate Particles by Co-Bipy "scalpel" for High Efficiency Thermal Decomposition. *Adv. Sci.* **2022**, *9*, 2204109. [CrossRef]
43. Chaturvedi, S.; Dave, P.N.; Patel, N.N. Thermal decomposition of AP/HTPB propellants in presence of Zn Nanoalloys. *Appl. Nanosci.* **2015**, *5*, 93–98. [CrossRef]
44. Zhu, G.; Tan, J.; Tan, L.; Wu, Q.; Ren, X.; Fu, C.; Chen, Z.; Meng, X. Growth of CeCo-MOF in dendritic mesoporous organosilica as highly efficient antioxidant for enhanced thermal stability of silicone Rubber. *Chin. Chem. Lett.* **2025**, *36*, 109669. [CrossRef]
45. Gao, Q.; Li, J.; He, Y.; Zhao, J.; Li, J.; Shao, D.; Wang, M.; Hu, J. High-performance antioxidant behavior of zeolitic imidazolate framework-67 at low filler content in silicone Rubber. *Polym. Degrad. Stab.* **2021**, *190*, 109622. [CrossRef]
46. Rocco, J.A.F.F.; Lima, J.E.S.; Frutuoso, A.; Iha, K.; Ionashiro, M.; Matos, J.; Suárez-Iha, M. TG studies of a composite solid rocket propellant based on HTPB-Binder. *J. Therm. Anal. Calorim.* **2004**, *77*, 803–813. [CrossRef]
47. Ma, T.; Wang, W.; Wang, R. Thermal Degradation and Carbonization Mechanism of Fe-Based Metal-Organic Frameworks onto Flame-Retardant Polyethylene Terephthalate: 1. *Polymers* **2023**, *15*, 224. [CrossRef] [PubMed]
48. Zhou, P.; Ren, Z.; Tang, X.; Zheng, Z.; Zhang, K.; Liao, J.; Zhong, Y.; Zhang, Y.; Huang, C. Interaction Between Prussian Blue Ultrathin Nanosheet and Ammonium Perchlorate for Highly Efficient Thermal Decomposition. *Adv. Funct. Mater.* **2023**, *33*, 2300661. [CrossRef]
49. Hu, Y.; Tao, B.; Shang, F.; Zhou, M.; Hao, D.; Fan, R.; Xia, D.; Yang, Y.; Pang, A.; Lin, K. Thermal decomposition of ammonium perchlorate over perovskite catalysts: Catalytic decomposition behavior, mechanism and Application. *Appl. Surf. Sci.* **2020**, *513*, 145849. [CrossRef]
50. Wang, Y.-H.; Liu, L.-L.; Xiao, L.-Y.; Wang, Z.-X. Thermal decomposition of HTPB/AP and HTPB/HMX mixtures with low content of Oxidizer. *J. Therm. Anal. Calorim.* **2015**, *119*, 1673–1678. [CrossRef]